

Gaussianity revisited: Exploring the Kibble-Zurek mechanism with superconducting rings

D J Weir¹, R Monaco², V P Koshelets³, J Mygind⁴
and R J Rivers⁵

¹ Helsinki Institute of Physics, Gustaf H  llstr  min katu 2a, 00014 Helsinki, Finland

² Istituto di Cibernetica del CNR, Comprensorio Olivetti, 80078 Pozzuoli, Italy
and Facolt   di Scienze, Universit   di Salerno, 84084 Fisciano, Italy

³ Kotel'nikov Institute of Radio Engineering and Electronics, Russian Academy of
Science, Mokhovaya 11, Bldg 7, 125009 Moscow, Russia.

⁴ Department of Physics, B309, Technical University of Denmark, DK-2800 Lyngby,
Denmark.

⁵ Blackett Laboratory, Imperial College London, London SW7 2AZ, U.K.

E-mail: david.weir@helsinki.fi

Abstract. In this paper we use spontaneous flux production in annular superconductors to shed light on the Kibble-Zurek scenario. In particular, we examine the effects of finite size, and of external fields, neither of which is directly amenable to the KZ analysis. We see, from extensive simulations, that a realistic 2D superconducting annulus in 3D space, with dynamical electromagnetic fields behaves very like, and often indistinguishably from, a 1D ring with classical EM fields. Further, the properties of that 1D ring are well represented by analytic Gaussian approximations. Experimental results for annuli in the presence of external fields confirm these numerical findings, which have implications for the relevance of causal horizons to determine defect production.

PACS numbers: 05.70.Fh, 11.27.+d, 74.50.+r

Submitted to: *J. Phys.: Condens. Matter* issue ‘Condensed Matter Analogues of Cosmology’

1. Introduction

Causality imposes constraints on systems that are strongly out of equilibrium by restricting the rate of change of correlation lengths to the relevant causal speed (such as the speed of sound). This is particularly the case in the vicinity of symmetry-breaking continuous transitions where, adiabatically, correlation lengths become arbitrarily large. Since such transitions take place in finite time, correlation lengths must remain finite. The faster the transition rate and the shorter the time available for system ordering, the more constrained the correlation lengths will be.

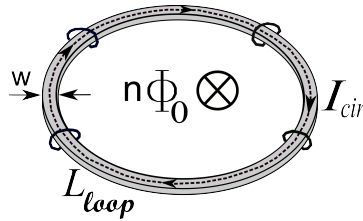


Figure 1. 3D sketch (not to scale) of a superconducting ring of width w with n trapped magnetic flux quanta, in the absence of any external flux. The dashed line indicates that a supercurrent, I_{cir} , circulates around the ring. The magnetic field (solid) lines wrap around the ring section.

The suggestion that causality would constrain correlation lengths was originally made by Kibble[1, 2] in the context of the very early universe. The relevance for the early universe is that if the system is frustrated this is relieved by the spontaneous creation of topological defects, whose separation reflects the correlation lengths at the time of their appearance, and which should be visible today. Zurek[3, 4] independently reached the same conclusions for condensed matter systems in what is known as the Kibble-Zurek (KZ) scenario.

This paper focuses on the behaviour of superconducting annuli. We follow Zurek in considering spontaneous flux production arising from rapid temperature quenches into the superconducting phase as a result of constrained correlation lengths. An idealisation of our experimental setup – which we shall discuss later – is shown in Fig.1. Further details are given in the appendix.

To model the system we assume a simple complex scalar field $\phi(x)$ that can act as a proxy for a Cooper pair, decomposed as

$$\phi(x) = |\phi(x)|e^{i\theta(x)}. \quad (1)$$

For the sake of argument we restrict ourselves to the inner radius of the annulus, where x measures the distance along the ring, circumference C . On quenching from the normal to the superconducting phase, we can define a winding number density $n(x) = \partial_x \theta(x)/2\pi$ along this circumference. In the absence of any external fields the total winding number n around the loop is zero on average, but will have non-zero variance

$$\langle n^2 \rangle = \int_0^C dx \int_0^C dy \langle n(x) n(y) \rangle, \quad (2)$$

and it is this that we measure, indirectly, through the matching flux generated in the interior of the annulus, which is directly observable. This flux is quantised (as fluxoids) in units of $\Phi_0 = hc/2e$.

For large annuli, for which $C \gg \bar{\xi}$, we can replace (2) by

$$\langle n^2 \rangle = \frac{C}{2} \int_0^C dx \langle n(x) n(0) \rangle \approx \frac{C}{2} \int_0^\infty dx \langle n(x) n(0) \rangle, \quad (3)$$

if we assume that the two-point correlation function $\langle n(x) n(y) \rangle$ is of short range compared to C . Suppose the correlator is described through the single length scale

$\bar{\xi}$. Simple dimensional analysis then gives

$$\langle n^2 \rangle = a \frac{C}{\bar{\xi}} \quad (4)$$

for $\bar{\xi}$ of (5). This is the perimeter law assumed in the Kibble-Zurek picture, interpreted as a random walk in phase along the circumference in steps of length $\bar{\xi}$. The same analysis would apply to spontaneous superflow in an annular tube of superfluid ^4He [4] but whereas it is difficult to perform such a measurement there, in our case we can measure the flux directly to determine the characteristic correlation length.

To estimate the length scale $\bar{\xi}$ we repeat the Kibble-Zurek argument of [3, 4], assuming rapid cooling through a continuous transition, transition temperature T_c . Suppose $\xi(t)$ is the *adiabatic* correlation length for $n(x)$ at time t , diverging at the transition at $t = 0$ as the temperature $T(t)$ changes ($T(0) = T_c$). If the system is initially homogeneous and isotropic the KZ scenario proposes that on approaching the transition the increasing correlation length, originally changing adiabatically, will freeze (the ‘impulse’ regime) at time $t_< < 0$, when $\dot{\xi}(t_<) \approx c(t_<)$, where $c(t)$ is the relevant causal speed at time t . After passing through the transition the system will unfreeze into a new adiabatic regime at a time $t_> > 0$ when $|\dot{\xi}(t_>)| \approx c(t_>)$. The correlation length $\bar{\xi}$ that sets the scale for phase change along the ring is

$$\bar{\xi} \approx \xi(t_>) = \xi_0 \left(\frac{\tau_Q}{\tau_0} \right)^\sigma, \quad (5)$$

where ξ_0 and τ_0 are system-dependent and τ_Q is the quench time (the inverse quench rate through the transition). The exponent σ can be derived from critical exponents valid for the adiabatic transition and the out-of-equilibrium behaviour is thereby categorised by the equilibrium universality class of the system. For Type-II superconductors $t_> = \sqrt{\tau_0 \tau_Q}$ and $\sigma = 1/4$ in the mean-field approximation.

There is a somewhat different viewpoint, predicated on the approximate Gaussianity of fast quenches, explored several years ago by one of us (RR) [5, 6]. More recently, preliminary simulations which further support underlying Gaussian behaviour were performed by us [7, 8] and this paper continues this analysis in two ways. Firstly, we extend both the numerical simulations and the analytical approximations to see more closely the validity of simple Gaussian assumptions. Secondly we present new experimental data on the presence of fluxoid production in the presence of an external field, which go beyond the reach of the KZ scenario, but for which Gaussian assumptions give predictions.

Our starting point is the observation that we would get the same scaling behaviour (5) if we evaluated ξ at $t_<$ and, indeed, it has been proposed that $t_<$ is as relevant a time as $t_>$ [2, 3], but we know for other reasons that it is what happens after the transition is implemented that determines the relevant distance scales [9]. This suggests defect formation as due to the growth of unstable long wavelength modes as the field is rolling off the hill which now denotes the unstable symmetry preserving vacuum, rather than through direct causal bounds. If, nonetheless, we take the KZ scenario as a guide

for the time $t_>$ at which defects form, then $t_>$ is much smaller than the time it takes for the order parameter field(s) to experience the degenerate vacua. If they remain so close to the unstable 'vacuum' that the non-linearities of the backreaction can be approximately ignored then the effectively linearised field equations give rise to Gaussian field correlation functions. Generally, these lead to the identical scaling behaviour (1) for fast quenches for large systems, both non-relativistic and relativistic [5, 6]. In practice, whatever the difference in language, our viewpoint is not very dissimilar from the KZ picture, in that both our simulations and the many simulations (e.g. [10, 11, 12]) demonstrating the validity of the scaling behaviour (5) are based on *time-dependent* Ginzburg-Landau (TDGL) theory. It is these equations that we linearise to derive the Gaussian results.

Having said that, there are two issues which force us to step outside the KZ picture and it is here that the greater generality of our approach is crucial. The first is that, whereas the early universe can be taken as homogeneous to a very high degree, the same cannot be said about laboratory systems. One step to limit inhomogeneity is to make the systems small. However, this looks to be swapping one problem for another in that we have now incurred finite size effects. Specifically, the scaling behaviour (5) assumed that $C \gg \bar{\xi}$. The Gaussian approximation permits an analytic replacement to (4) and (5) for *homogeneous* small systems for which $C < \bar{\xi}$ which is inaccessible to the KZ picture. Thus, what seems to be a problem is, in fact, an opportunity. We can use small annuli to cast the KZ scenario in a different light and illuminate the Gaussian approximation.

Secondly, the Gaussian approximation has a further reach, to explicit symmetry breaking driven by the application of external fields, for which the KZ scenario again offers little help. This is an interesting problem in its own right and experimentally is a serious problem because of the presence of stray fields in the laboratory. Scaling behaviour (5) can only be demonstrated once external fields have been countered upon which, again, the Gaussian approximation gives insight.

This paper is organised as follows. For narrow rings we might hope that the system behaves one-dimensionally. In the next section we reexamine the Gaussian approximation (or rather, two closely related Gaussian approximations) both for large and small idealised 1D systems. We shall show later that numerical simulations provide strong support for Gaussian behaviour, both in the power spectrum of field ordering and in the damping of fluxoid generation in small systems, an exercise begun in [7, 8] and developed considerably here. In particular, we explore the way the power of field fluctuations is driven into long wavelengths through the growth of unstable modes, in good accord with our Gaussian expectations.

In the subsequent sections we briefly summarise earlier work of ours [8] in which we simulated a 2D superconducting annulus embedded in 3D space, with a fully dynamical electromagnetic field in three dimensions. The reader is referred to that paper for further details. Surprisingly, we found that our results are, in key ways, indistinguishable from those of the 1D simulation and thereby, of the Gaussian approximation.

We conclude with a discussion of new experimental results for fluxoid production in an external field and show that it too, is explicable in terms of Gaussian fluctuations. As we said earlier, the experimental details are given in the appendix.

2. Gaussian behaviour for 1D systems

Unsurprisingly, 1D systems are the easiest for which to make analytic predictions and to implement numerical simulations. There are two strongly related variants of Gaussian approximation that we shall consider; each has its strengths.

2.1. Long superconductors: Gaussian probabilities

Our first Gaussian approximation, first proposed in [13, 14], has the advantage of being much simpler analytically, predicated on the perimeter rule (4). We begin by considering a large loop, divided up into N domains, in each of which θ is a constant. We assume that there is no correlation between the values of θ in adjacent domains but, in calculating the phase change $\Delta\theta$ for the loop, the geodesic rule is adopted. This means that the shortest path in phase will be taken when jumping from one domain to the other.

Let $G_N(\Delta\theta)$ be the probability that the change in phase θ is $\Delta\theta$ after the N links that make the loop. The assumed lack of correlation means that the probability of ending with a phase shift of $2\pi m$ (i.e., net fluxoid number m) is:

$$p_m(N) = \int_{-\pi+2m\pi}^{\pi+2m\pi} d\Theta G_N(\Theta). \quad (6)$$

It follows that $p_m(N) = p_{-m}(N)$.

To bring this into correspondence with the KZ scenario, we should identify the domain size as comparable to $C/\bar{\xi}$, i.e., $C = aN\bar{\xi}$, where $a = O(1)$. With this in mind, we assume that the total phase change $\Delta\theta$ around the loop can be expressed as the sum of a random term Θ and a geodesic-rule correction $\delta\Theta$, necessary to obtain an integer winding number [15]. It is convenient to relax N to be a *continuous* variable. We further assume that Θ has a normal distribution with average $\bar{\Theta} = 0$ and variance σ^2 proportional to N i.e.,

$$G_N(\Theta) = \frac{1}{\sqrt{2\pi\sigma^2(N)}} \exp -\frac{\Theta^2}{2\sigma^2(N)}. \quad (7)$$

The trapping probabilities $p_m = p_{-m}$ are easily found: In particular, since in our experiments we rarely see more than one fluxoid, we are primarily interested in

$$p_0(N) = \text{erf}\left[\frac{\pi}{\sqrt{2\sigma^2(N)}}\right] \quad (8)$$

and

$$\bar{p}_1 = p_1(N) + p_{-1}(N) = \left[\text{erf}\frac{3\pi}{\sqrt{2\sigma^2(N)}} - \text{erf}\frac{\pi}{\sqrt{2\sigma^2(N)}} \right]. \quad (9)$$

From the large- N behaviour of the p_m it follows that, for large rings, $\sigma^2(N) = 4\pi^2\langle n^2 \rangle$. Also, we can identify Eq. (7) from the central limit distribution by taking $\sigma^2(N) = \frac{\pi^2}{3}N$ for large N . Further details may be found in Ref. [15].

2.2. A Gaussian variant: Gaussian distributions

We stay with large annuli but, rather than assume the Gaussian distribution for Θ of (7) we assume that the winding number density field $n(x)$ is a Gaussian field. It then follows that the all important probabilities of finding no fluxoids or one fluxoid are

$$f_0 = \frac{1}{2\pi} \int_{-\pi}^{\pi} dz \exp(-z^2 \langle n^2 \rangle / 2) \quad (10)$$

and

$$\bar{f}_1 = f_1 + f_{-1} = \frac{1}{\pi} \int_{-\pi}^{\pi} dz \exp(-z^2 \langle n^2 \rangle / 2) \cos z \quad (11)$$

respectively. We use the notation f_m for the probability of winding number m in this approximation to distinguish it from the p_m of the previous section for Gaussian winding number densities. Neither (8) or (9) take periodicity into account.

In Fig. 2 we show how the predictions for p_n and f_n are almost indistinguishable once we get away from very small probabilities where periodicity is important. Further, we see that, with that caveat, they agree with the simulations for the fully interacting theory, discussed below. In particular, the Gaussian upper bound on finding a single fluxoid at about 0.49 that follows from (8) or (9) is saturated in the simulation (within errors). This supports the Gaussian approximation in its simplest guise.

The Gaussian approximations so far do not give the KZ scaling behaviour of (5). To see this we make the further Gaussian approximation that, on decomposing the complex order parameter field as $\phi = (\phi_1 + i\phi_2)/\sqrt{2}$, ϕ_1 and ϕ_2 are independent Gaussian fields. The correlation function for the winding number density is now determined by the correlation function $G(x)$ for the field components, defined by

$$\langle \phi_a(x) \phi_b(y) \rangle = \delta_{ab} G(|x - y|). \quad (12)$$

We now use the fact that, for damped systems, the Gaussian approximation corresponds to a linearisation of the time-dependent Ginzburg-Landau (TDGL) equations. Periodicity is unimportant for large rings and we find that, for the linear TDGL equations [16], field correlation functions $G(r)$ at the defect formation time for large systems take the form ($r = |\mathbf{x}|$)

$$G(r, t) = \int d\mathbf{k} e^{i\mathbf{k} \cdot \mathbf{x}} P(k, t) \quad (13)$$

in which the power spectrum $P(k, t)$ has a representation in terms of the Schwinger proper-time τ (in the dimensionless units of (26) below) as (approximately) [5, 6, 16]

$$P(k, t) \propto \int_0^\infty d\tau e^{-\tau k^2} e^{-\int_0^\tau ds \epsilon(t-s/2)} \quad (14)$$

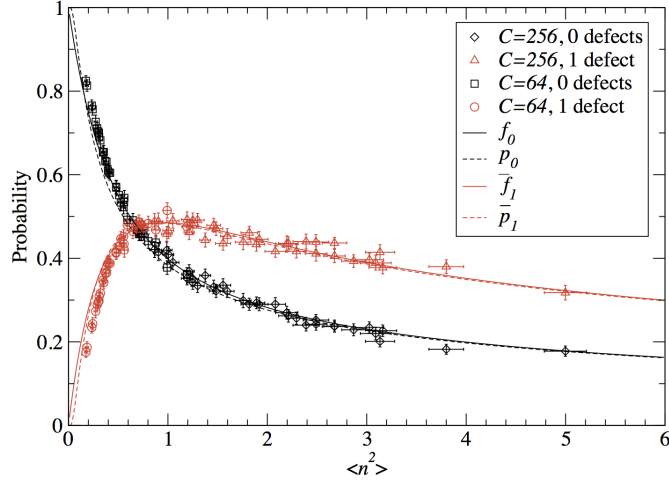


Figure 2. We plot (p_0, f_0) and then (\bar{p}_1, \bar{f}_1) against $\langle n^2 \rangle$ for a 1D superconducting ring to show the similarity of the Gaussian approximations. In particular, both \bar{p}_1 and \bar{f}_1 have maximum values of approximately 0.49. Both are contrasted with the results of the 1D simulation derived from (26). Because neither approximation takes periodicity into account the likelihood of seeing flux at low levels is overestimated; see Fig. 5. Otherwise agreement is good within errors.

where $\epsilon(t) \equiv T(t)/T_c$ is the reduced temperature. We assume the dependence $\epsilon(t) = -t/\tau_Q$ for a quench linear in time in the vicinity of the phase transition where fluxoid formation takes place. Adopting this $\epsilon(t)$ gives

$$P(k, t) \propto \int_0^\infty d\tau e^{-\tau k^2} e^{t\tau/\tau_Q} e^{-\tau^2/4\tau_Q} \quad (15)$$

$P(k) \propto k^{-2}$ for large k^2 . In the dimensionless units above, the time for the formation of fluxoids is $t_> = O(\sqrt{\tau_Q})$.

There is a note of caution. 1D systems have some peculiarities (such as the fact that formally there are no transitions in 1D). In D spatial dimensions the integration variable ϕk of (13) is replaced by $\phi^D k$. When $D \geq 2$ the integral is dominated by the ultraviolet for slow quenches, which needs to be cut off at distance scale ξ_0 .

To convert the Gaussian behaviour of the fields into the Gaussian behaviour of the winding number density is a messy process. A simple approximation, sufficient for our purposes, gives [7]

$$\langle n(x) n(0) \rangle \approx \frac{2}{(2\pi)^2} [f'(x)^2 - f''(x) f(x)] \quad (16)$$

where $f(x) = G(x)/G(0)$.

For $D = 1$ or provided quenches are fast enough that we can ignore the ultraviolet effects then, evaluated at the KZ time $t_> \approx \tau_Q^{1/2}$, $f(r)$ ($r = |x|$) takes the Gaussian form

$$f(r) \approx e^{-r^2/2\xi_r^2} \quad (17)$$

for *small* r , where $\xi_r \approx \bar{\xi}$, the KZ separation length [5, 6]. This is appropriate for a damped system at *short* distance.

This creation of winding number can be thought of as due to the unstable long wavelength modes of the field growing as fast as possible, with no backreaction in the short time necessary. It follows that

$$\langle n^2 \rangle \approx a \frac{C}{\xi_0} \left(\frac{\tau_Q}{\tau_0} \right)^{-\sigma}, \quad (18)$$

where $\sigma = 1/4$.

All the above ignores periodicity. The advantage of choosing Gaussian fields is that they permit periodic boundary conditions in a way that the Gaussian distributions as posed above do not.

2.3. Small annuli: Gaussian approximation

We would expect that small systems, whether superconductors or not, would show proportionately less defect production per unit length than larger systems because of end effects or periodicity. Let us consider small annuli for which $C/\bar{\xi} \ll 1$.

The periodicity of $f(x)$ in $x \pmod{C}$ is now important. The effect of periodicity is to discretise k in (15). To implement this in the approximation (17) we need to replace $f(x)$ by its periodic generalisation, the Jacobi ϑ function [7]

$$f(x)_{per} = \frac{\vartheta_3(\pi x/C | 2\pi i \xi_r^2/C^2)}{\vartheta_3(0 | 2\pi i \xi_r^2/C^2)} \quad (19)$$

$$\approx 1 - 4 \sin^2(\pi x/C) e^{-2\pi^2 \xi_r^2/C^2}, \quad (20)$$

whence, from (2),

$$\langle n^2 \rangle = \mathcal{O}(e^{-4\pi^2 \xi_r^2/C^2}). \quad (21)$$

Thus, rather than the power falloff for large loops we have exponential damping

$$\ln \langle n^2 \rangle \approx -4\pi^2 \xi_r^2/C^2 + \text{const.} \quad (22)$$

Since it is small, $\langle n^2 \rangle \approx f_1$, the probability of finding single winding number along the annulus.

In principle $\xi_r \propto \tau_Q^\sigma$, but some caution is necessary in that the approximation of (16) is oversimple, which makes the single term (22) only approximate. In [7] we showed that exponential damping does take place. However, we can go further in that, if we combine (18) for $\sigma = 1/4$ with (22), it follows that

$$\langle n^2 \rangle = F(\tau_Q/C^4) \quad (23)$$

for some universal function F interpolating between power behaviour and exponential damping that covers all sized annuli and quench rates.

2.4. Numerical simulations

We simulate our 1D superconductor with the U(1) scalar field theory of the complex order parameter ϕ , given previously, on a ring of circumference C with periodic boundary conditions. There is no way to include a dynamical electromagnetic field in a 1D simulation. To mimic a temperature quench through its critical point at time $t = 0$ we take an explicitly time-dependent potential

$$V(|\phi|^2) = \epsilon(t)|\phi|^2 + \frac{1}{2}b|\phi|^4. \quad (24)$$

Rather than just take ϵ linear in t , as we did in (15), we now adopt the more realistic behaviour

$$\epsilon(t) = \begin{cases} 1, & t < -\tau_Q \\ -t/\tau_Q, & -\tau_Q < t < \tau_Q \\ -1, & t > \tau_Q \end{cases}, \quad (25)$$

to model a slow quench, in which the quench has a beginning and an end. We start at $t = -2\tau_Q$ and continue until $t = 4\tau_Q$, by which time the defects have frozen out. This system is modelled by a damped second-order Langevin equation,

$$\partial_t^2 \phi_a - \partial_x^2 \phi_a + \eta \partial_t \phi_a + \frac{\partial V}{\partial \phi_a} = \zeta_a, \quad (26)$$

with zero mean Gaussian noise for which

$$\langle \zeta_a(x', t') \zeta_b(x, t) \rangle = 2\eta T \delta(x' - x) \delta(t' - t) \delta_{ab}. \quad (27)$$

The interaction strength b is taken to be unity and we take $\eta = 1$ and $T = 0.01$, yielding a heavily damped system.. Our linearised Gaussian approximations are independent of b in the first instance. A mean-field generalisation of the Gaussian approximation in which the self-interactions are also linearised does give a weak b -dependence (e.g. see [5]). We have performed our simulations for larger values of b without any noticeably different results. In evolving the equations a stochastic leapfrog method is used [17]. Further details may be found in Ref. [7].

Our first application of this simple simulation in the current work is to test the validity of our Gaussian approximations discussed earlier. In Fig. 2 we show the observed frequencies for trapping a given number of fluxoids as a function of $\langle n^2 \rangle$. This is compared with the Gaussian predictions (p_0, f_0) and (\bar{p}_1, \bar{f}_1) . Agreement is surprisingly good – at least for sufficiently large $\langle n^2 \rangle$.

In Fig. 5 we compare the simulation results, scaled according to Eq. (23), for $\langle n^2 \rangle$ as a function of quench time. The transition from KZ scaling to exponential suppression is very clear.

As we saw above, we have $G(0) \propto \int dk k^{D-1} P(k)$; it and other moments of $P(k)$ play an important role in winding number evolution [18]. In Fig 3 we take the first moment

$$I(t) = \frac{\int_0^{2\pi} dk k P(k)}{\int_0^{2\pi} dk P(k)} \quad (28)$$

for a given τ_Q . The cutoff $k = 2\pi$ corresponds to a length cutoff at $O(\xi_0)$ in our dimensionless units. In Fig. 3 (a) we plot $kP(k)$ from the numerical simulation for $t > 0$ in multiples of $\sqrt{\tau_Q}$. As we expect, the power gets pushed into longer and longer wavelengths as the field becomes ordered. The scale over which that is ordered becomes clearer in the moment $I(t)$ of (b), in which we compare the simulation to the analytic behaviour of (15). The expression (15) corresponded to an unbounded linear quench without the brakes imposed for $|t| > \tau_Q$ of (25). The comparison to simulations is only valid for $t > -\tau_Q$, where it is seen to be good. As it stands the Gaussian approximation drives the power to longer wavelengths than the simulation but, as we know from elsewhere [16], the scaling behaviour of the dominant wavelength (corresponding to $\bar{\xi}^{-1}$) still satisfies the same scaling behaviour as for the simulation for large annuli.

We also find that, provided the time is not too late, the diagonalisation of (12) in field components is approximately satisfied, but with large noise; we do not present any data to that effect.

3. Simulations of Annular superconductors in three dimensions

Even thin annuli are not one-dimensional and we should take the annulus width into account. Moreover, to compound the problem, even a superconductor that is effectively a 2D film cannot be treated entirely as two-dimensional. The three-dimensional nature of the flux lines cannot be ignored. In fact, the KZ analysis is known to be incomplete, in that the possibility exists of long wavelength modes of the electromagnetic field freezing in as the transition is implemented. We have seen elsewhere [8] that this secondary mechanism, the Hindmarsh-Rajantie (HR) mechanism [19, 20], does not seem to be important for our small systems and we shall not pursue it further.

3.1. The 2D Gaussian approximation

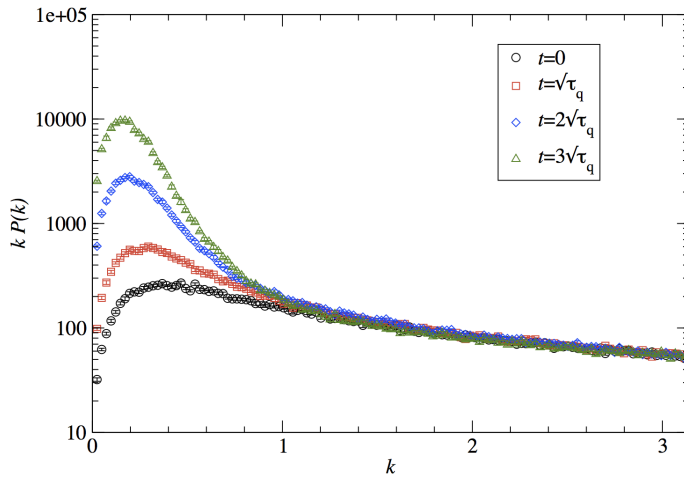
For the moment we restrict ourselves to the complex field $\phi_a(\mathbf{x})$, extended now to the $x_1 - x_2$ plane, assumed Gaussian, as before. As it stands it is too difficult to get analytic results for arbitrary annuli so, as a first step, we consider a 2D superconducting film of infinite extent and we look for the behaviour of the winding number along a circular closed loop in the film of circumference C , that encloses a surface S .

If the topological density [21, 22] in the plane is $\rho_3(\mathbf{x})$, for given field configurations $\phi_a(\mathbf{x})$ the phase change θ_C along the path can be expressed as the surface integral

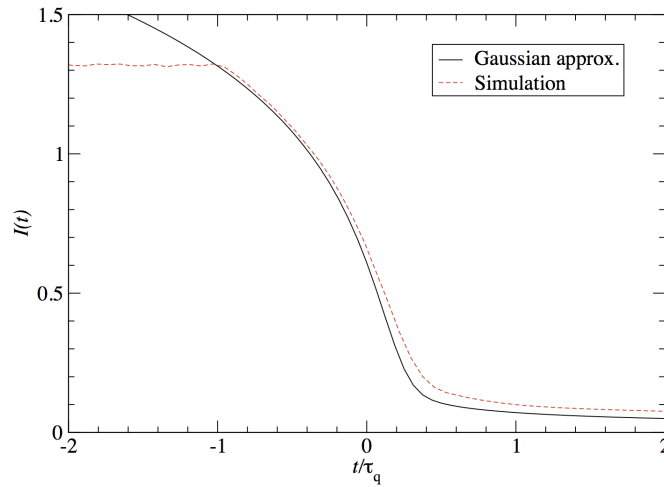
$$\theta_C = 2\pi \int_{\mathbf{x} \in S} d^2x \rho_3(\mathbf{x}) = -2\pi \int_{\mathbf{x} \notin S} d^2x \rho_3(\mathbf{x}) \quad (29)$$

from charge conservation. It then follows from the results of Refs. [21, 22] that, for Gaussian fields, $\langle n^2 \rangle$ satisfies

$$\langle n^2 \rangle = - \int_{\mathbf{x} \notin S} d^2x \int_{\mathbf{y} \in S} d^2y \langle \rho_3(\mathbf{x}) \rho_3(\mathbf{y}) \rangle, \quad (30)$$



(a)



(b)

Figure 3. (a) We plot $kP(k)$ against k for a variety of $t > 0$, in multiples of the KZ time $t_{>} = \sqrt{\tau_Q}$ for $\tau_Q = 32$ on a lattice of size $C = 256$. The characteristic wavelength increases with increasing time as the field orders itself. Details of the quench are given below. (b) We plot the first moment of $P(k)$ from the simulation and compare it to its value from (15). The comparison is only valid for $t > -\tau_Q$, where it is good. We note that an identifiable scaling length is only established for $t \gtrsim 3t_{>}$. This is reasonable from the KZ viewpoint since $t_{>}$ is the *minimum* time at which the system could unfreeze.

where \mathbf{x} and \mathbf{y} are in the plane of S . It is not difficult to express the density correlation in terms of the field correlation $f(r)$ ($r = |\mathbf{x}|$),

$$\langle \rho_3(\mathbf{x}) \rho_3(\mathbf{0}) \rangle = \frac{1}{4\pi^2 r} \frac{\partial}{\partial r} \left(\frac{f^2(r)}{1 - f^2(r)} \right). \quad (31)$$

It follows from (17) that the density correlation has a range $O(\xi_r)$. With \mathbf{x} outside S , and \mathbf{y} inside S , all the contribution to $\langle n^2 \rangle$ comes from the vicinity of the boundary of S , rather than the whole area. For large rings this means that, if we removed all material except for a strip of width $O(\bar{\xi})$ from the neighbourhood of the contour C we would still have the same result. As before, this gives the perimeter rule

$$\langle n^2 \rangle \approx a' \frac{C}{\xi_r}. \quad (32)$$

That is, we have the anticipated random walk in phase along the contour, from which we recover the canonical scaling (5) on identifying ξ_r .

We can say more. The analysis that led to the expressions (14) and (15) for the power spectrum of the fluctuations is dimension independent and only depends on the Gaussian nature of the fields. Dimension only arises in the construction (13) for the correlation functions, and we shall not repeat the simulations in this case.

For small annuli the situation is less clear. While the behaviour of (30) suggests that the winding number along a small closed path in a 2D superconducting film is proportional to the area of the ring (and hence doubles the KZ exponent), it is not clear that this behaviour would be preserved if the interior of the closed path were removed to make a broad annulus. A test of this is to preserve the perimeter of the annulus but to take different aspect ratios (i.e. different areas). A perimeter law would leave probabilities unchanged, but an area law would lead to differences. The relevance of this is that in an earlier experiment [23], results suggested a doubling of the KZ exponents – albeit with large errors. We shall return to the question of exponent doubling for small systems in our conclusions.

3.2. Simulations

To test the approximations outlined in the previous sections we have simulated the system illustrated in Figure 4, in which the superconducting ring (where the complex scalar field ϕ is defined) is surrounded on all sides by a box in which the standard U(1) vacuum electrodynamics is simulated. Although the superconductor is thereby taken to be a thin planar film, the three-dimensional simulation allows for nontrivial correlations of the magnetic field. Details are given in [8], to which we refer the reader, and we only summarise them here.

Extending the approach used for the 1D ring, we use the gauge-invariant Langevin formulation for gauge and scalar fields [24], denoting the lattice order parameter field again as ϕ and the gauge fields as A_i .

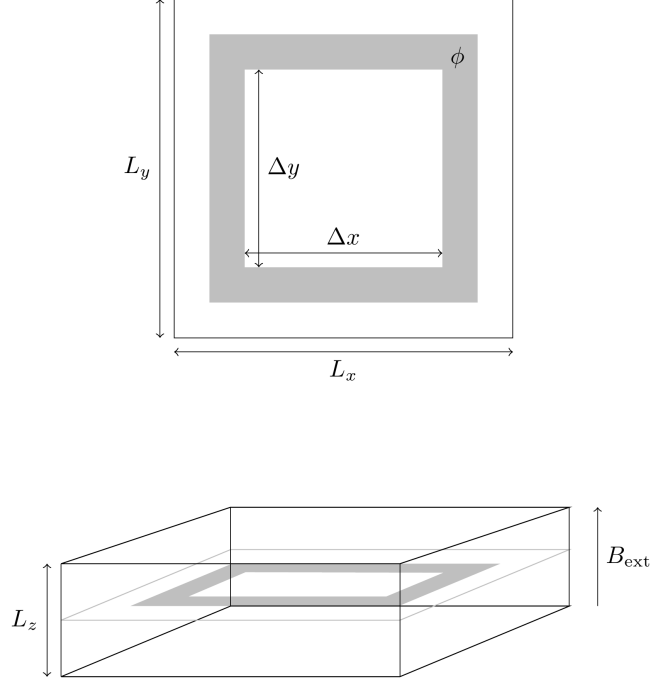


Figure 4. The 3D simulation consists of a thin superconducting ring (shown in grey) suspended in a box of size $30 \times 30 \times 5$. (we take $\delta x = 0.5$). The ring is of width 5, the borders also of thickness 5, while the square central void has size $\Delta x = \Delta y = 10$. An external magnetic flux density B_{ext} is applied, as shown. Periodic boundary conditions are used.

The Hamiltonian for the system is

$$\begin{aligned}
 H = & \frac{1}{2} \sum_{x,i} (\delta x)^3 \left[E_i(x)^2 + \sum_{jk} (\epsilon_{ijk} \Delta_j^+ A_k(x))^2 \right] \\
 & + 2 \sum_{x,i} \text{Re } \phi^\dagger(x) U_i(x) \phi(x+i) \\
 & + (\delta x)^2 \sum_x \left[\Pi^* \Pi + \left(\epsilon(t) + \frac{4}{(\delta x)^2} \right) \phi^\dagger \phi + \frac{1}{2} b (\phi^\dagger \phi)^2 \right]
 \end{aligned} \tag{33}$$

where $U_i(x) = e^{iaeA_i(x)}$, and the Δ^+ denote finite differences. Note that ϕ is only defined in a 2-dimensional superconducting film region; $\dot{\Pi}$ and \dot{A}_i are coupled in a gauge-invariant manner to Gaussian white noise with strength η . We will take $e = 0.1$ and $b = 0.1$, meaning we are simulating a type II superconductor with $\kappa = \sqrt{\lambda}/e \approx 3.2$. Periodic boundary conditions are used. The quench protocol is the same as for the 1D simulations, meaning $\epsilon(t)$ is of the form given in Eq. (25).

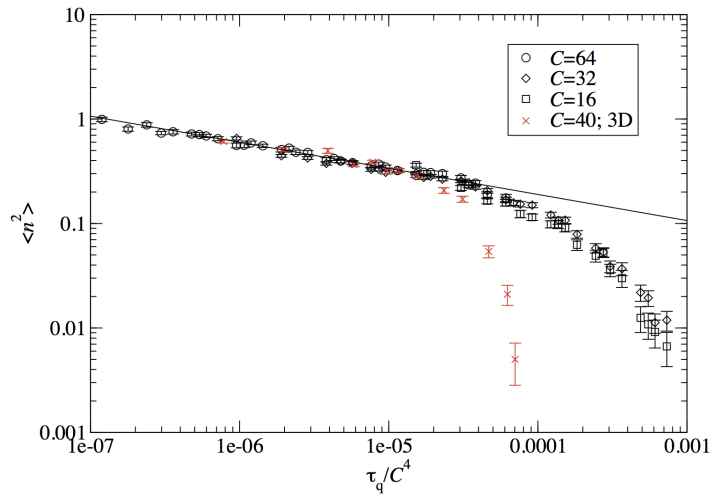


Figure 5. Results of simulations for annuli with inner circumference C in 1D and 3D, as a function of τ_Q/C^4 . The 1D simulations are represented by open symbols (black), the 3D by crosses (red). In the former case we see universal behaviour, and both a change in behaviour from KZ scaling to exponential suppression occurs. We see that there is complete agreement for large annuli (fast quenches) and different exponential damping for small annuli (slow quenches). A possible explanation for the difference lies in the way in which field correlations play a role in different dimensions.

Here, we first sought to see if the exponential falloff in trapping probability predicted above by 1D simulations persisted for the more realistic theory of 2D rings in three dimensions. We had in mind the possibility of exponent doubling, suggested earlier [23]. In Figure 5, we show the crossover from KZ behaviour to exponential damping as a function of the combination τ_Q/C^4 , for both the 1D and 3D systems discussed above.

Exhibiting universal behaviour of the form (23), the 3D data are represented by red crosses superimposed on 1D data for a variety of ring circumferences C . If we were to plot the same data on log-linear axes we would see that the collapse in probabilities is exponential (as we saw in 1D in [7]). However, while there is complete agreement for large annuli the different exponential damping for small annuli is dimension dependent. This is perhaps not surprising because of the differences between the 1D expression Eq. (16) and the 2D expression (31) on substituting Eq. (20) for $f(r)$, even though the annulus is not particularly wide [18]. As we would have anticipated, this difference is insensitive to self-coupling strength, as we have checked (but not displayed).

Further, in Ref. [8], differing aspect ratios were tried for the central hole for the same perimeter, ranging from a square to an elongated 5:1 rectangle, but no deviation from perimeter law behaviour (5) was detected, leading us to ignore the HR mechanism, whose contribution does not obey a perimeter law.

4. External fields

All the analysis above assumed no external fields. Experimentally, this is unrealistic. There are nearly always stray fields in the equipment or the environment. Moreover, driven symmetry breaking through the application of external bias is an interesting question in its own right. The KZ scenario cannot address this, but we shall find that we can obtain results in the Gaussian approximation that can be analysed in simulations.

Experimentally we compensate for unknown stray fields by applying an external bias field to cancel them. We know when this has happened when the likelihood of seeing spontaneous flux is at a minimum. To do this successfully we need to know the likelihood of fluxoid production in the presence of external fields. In practice it is difficult to extend the previous analysis with periodic boundary conditions to include external fields and we adopt a simpler straightforward variant of the Gaussian approximation.

4.1. Fluxoid production in an external field: 1D approximation

Let us now apply a magnetic flux Φ_f to the loop; this breaks the $\theta \rightarrow -\theta$ symmetry. The effect of Φ_f is to produce a non-zero average winding number $\langle n \rangle = \bar{n}(\Phi_f) = \Phi_f/\Phi_0$ after the transition, where $\Phi_0 = hc/2e$.

Because of the limitations of one dimension, the electromagnetic field can only be introduced classically. The natural extension [15] of our Gaussian probability model $G_N(\Theta)$ in Eq. (7) for a superconducting loop linked to a magnetic flux Φ_f is that the phase distribution will still be normal with the same variance $\sigma^2(N)$, but with non-zero average $\bar{\Theta}(\Phi_f) = 2\pi\bar{n}(\Phi_f) = 2\pi\Phi_f/\Phi_0 = 2\pi\phi_f$:

$$G_N(\Theta, \phi_f) = \frac{1}{\sqrt{2\pi\sigma^2(N)}} \exp - \frac{(\Theta - 2\pi\phi_f)^2}{2\sigma^2(N)} \quad (34)$$

With such a distribution, the probability p_m of ending up with a given winding number m is given by

$$p_m(\phi_f) = \int_{-\pi+2m\pi}^{\pi+2m\pi} d\theta G(\theta; \phi_f). \quad (35)$$

That is

$$p_{\pm m}(N, \phi_f) = \frac{1}{2} \left[\operatorname{erf} \frac{(\pm 2m - 2\phi_f + 1)\pi}{\sqrt{2\sigma^2(N)}} - \operatorname{erf} \frac{(\pm 2m - 2\phi_f - 1)\pi}{\sqrt{2\sigma^2(N)}} \right] \quad (36)$$

which, in the presence of a possible stray or residual flux ϕ_r , we reparametrise as

$$p_m(\phi_f) = \frac{1}{2} \left[\operatorname{erf} \frac{\phi_f - \phi_r - m + 0.5}{s_d} - \operatorname{erf} \frac{\phi_f - \phi_r - m - 0.5}{s_d} \right], \quad (37)$$

where the dependence on quench time and geometry is parameterised by $s_d \equiv \sqrt{2\sigma^2(N)/2\pi}$. Now, $p_{+m}(\phi_f) \neq p_{-m}(\phi_f)$. Essentially, what really matters is the difference $m - \phi_f$; for example, $p_m(1) = p_{m-1}(0)$. This calculation unfortunately does not allow us to determine the dependence of s on τ_Q . Nevertheless, we can fit data for different applied magnetic fields at fixed τ_Q to Eq. (37) with only s_d and ϕ_r as free

parameters to yield f_0 . We will test the validity of this ansatz (with $\phi_r = 0$) in our simulations.

We have seen that the Gaussian probability is a good approximation for large rings and, as before, we extrapolate to small rings, using (36) as it stands.

4.2. Simulations with an external field

Where we wish to impose an external field in our simulations, we do so by twisting a single plaquette – located at x_0 in the $x - y$ ($1 - 2$) plane. The effect of this, discussed in detail in Ref. [8], is to add the term

$$H_{\text{ext}} = a \sum_x (A_1(x) + A_2(x + a\hat{1}) - A_1(x + a\hat{2}) - A_2(x)) B_{\text{ext}} \delta^{(2)}(x - x_0) \quad (38)$$

to the Hamiltonian, where B_{ext} is the applied field, which can take arbitrary values because we have used the noncompact formulation of the gauge field A . Of course, the equations of motion must be modified to take account of this external field term. Results for nonzero external field are shown in Figure 6, with fits of the form in Equation (37) also shown. Despite the simple assumptions going into this ansatz, it agrees with the results of the simulations very well.

4.3. Experiments with an external field

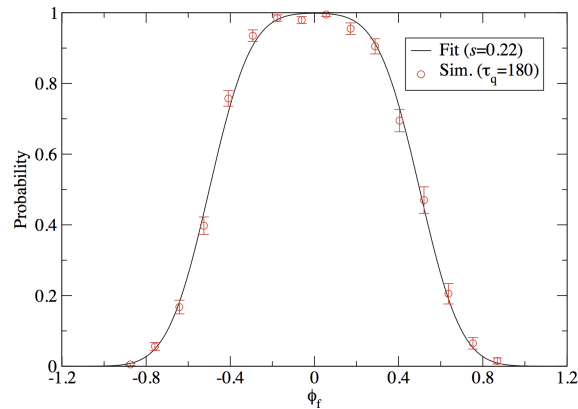
We have performed experiments using the setup of Fig. 1 to detect fluxoids produced in Nb annuli after a temperature quench in the presence of an external field. Details are given in the appendix. It is sufficient for the conclusion of this paper to say that the fluxoid probabilities match the simulations well which, in turn, means that they match the Gaussian form given in Eq. (37) extremely well. In Fig. 7 we give two examples of frequency dependency on the external field, for parameter values very similar to those shown in Fig. 6. Unfortunately, we do not have enough experimental data to show how \bar{p}_1 varies with τ_Q , except that it is in the exponentially suppressed regime.

5. Conclusions

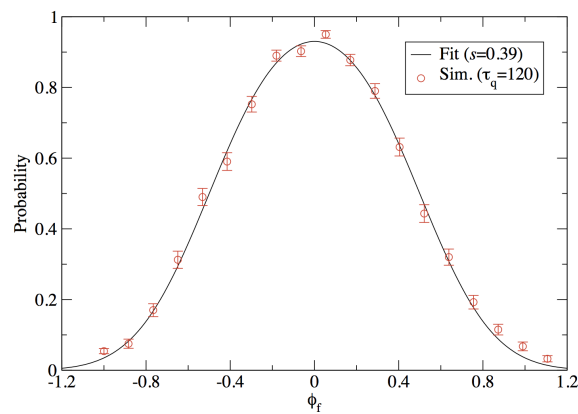
In this paper we have explored the ways in which spontaneous fluxoid production in annular superconductors can be used to cast light on the Kibble-Zurek (KZ) mechanism in systems that are far from equilibrium. In particular, does it represent the dynamics well?

With experiments both past and present in mind, the simple picture is complicated by two effects; small size and possible external fields. The KZ scenario is unable to address either of these. However, we know that the basic scaling results (5) also provide a good test of the Gaussian behaviour of the order parameter field and we have extended the Gaussian approximation to those areas which the KZ scenario cannot reach.

As it stands the Gaussian approximation is only simply analytic for an idealised 1D annulus, in which we can include an external magnetic field classically. In fact,



(a)

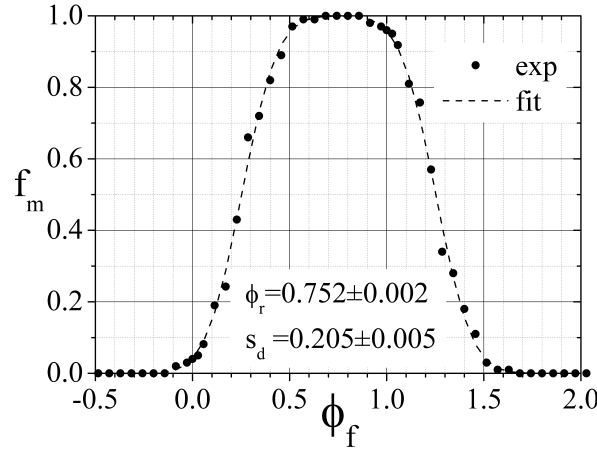


(b)

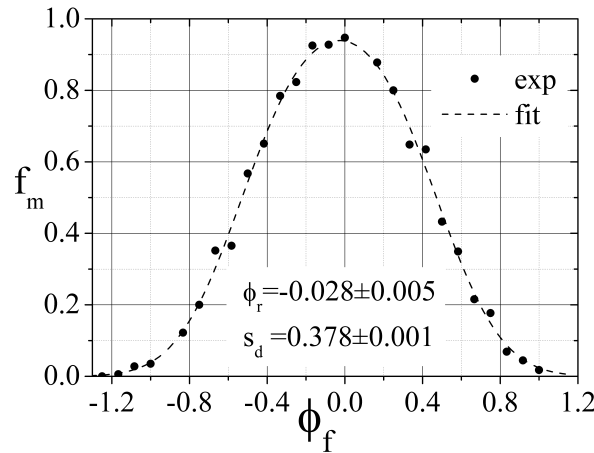
Figure 6. Simulated probability \bar{p}_1 of observing one defect as a function of normalised external magnetic flux ϕ_f for (a) $\tau_q = 180$ yielding $s = 0.22 \pm 0.01$ and (b) $\tau_q = 120$ corresponding to $s = 0.39 \pm 0.01$. The curves are a one-parameter fit to s of the form given in Eq. (37).

we have adopted two variants of Gaussianity which differ very slightly: one is more convenient for addressing periodicity, while the other for including external fields. We have performed simulations based on TDGL theory, both for the same idealised 1D annulus and for a more realistic annulus with finite width embedded in 3D space, in which the electromagnetic field is fully dynamical. Only in this latter case can we properly include the effects of external fields, necessary so that stray fields can be eliminated in experiment but interesting in its own right.

Our results are surprising. Where comparable, in major regards we find no important difference between the 1D and 3D simulations. In particular, the likelihood



(a)



(b)

Figure 7. Experimental probability \bar{p}_1 of observing onedefect as a function of normalised external magnetic flux ϕ_f . The curves are a fit of the form given in Eq. (37). The dashed lines show the best two-parameter fit to Eq.(37): (a) $\phi_r = 0.752$ and $s_d = 0.205$; (b) $\phi_r = -0.028$ and $s_d = 0.378$. The integer m is undetermined. These values are very close to those of Fig. 6 above. The experimental data, the simulated data and the Gaussian approximation for the probability are indistinguishable.

of fluxoid production depends only on the inner circumference of the annulus, and not on its shape, all other things being equal. For large rings we reproduce the canonical KZ scaling of (5). However, the likelihood of seeing fluxoids for small ring size or slow quenches is exponentially damped in a dimensionally dependent way. In the presence of the explicit symmetry breaking of external fields we find strong agreement between the 3D simulations and the 1D results of the Gaussian approximation. More to the point, we show experimental results for Nb annuli that agree totally with both.

The implications for the KZ scenario are strong. Rather than think in terms of

causal horizons as the constraints on growth of correlations, we see field ordering in terms of the fastest possible growth of unstable long wavelength modes, as seen both in the Gaussian approximation and in simulations. The validity of the Gaussian approximation as used here, and hence the scaling behaviour, is predicated upon damped TDGL equations describing the non-equilibrium dynamics of these modes, even though the KZ picture does not use this language in its *adiabatic* \rightarrow *impulse* \rightarrow *adiabatic* progression. In another paper in this volume one of us (RR) has shown that a cold tunable condensate can pass through the same sequence of freezing - unfreezing, whose causal bounds constrain correlation lengths. Although the KZ picture would suggest the formation of defects (vortices) in this case the absence of a supporting Gaussian approximation mitigates against this. Numerical simulations of this system are underway.

We conclude with an important issue that really requires a greater analysis. This is the empirical observation of scaling behaviour in which the observed exponents initially take *double* the canonical KZ values, as seemed to be the case in our earlier experiment on superconducting annuli [23] and as happened in our experiments on annular Josephson tunnel junctions [25, 13]. Further, a recent experiment on defect production in linear ionic crystals again shows twice the expected exponent [26]. We believe there are different reasons for all of these. In [23] we provided a possible Gaussian explanation for superconductors in terms of small size effects, which explanation was picked up by the authors of [26]. Preliminary analyses here suggest something more complicated. As we have seen above, the conditions we imposed in [23] for doubling in 1D systems are not satisfied for superconducting loops. Unless there is an effect due to annulus width (which Gaussianity suggests for wide annuli but which we have been unable to reproduce in simulations) our ‘doubling’ of [23], with its large errors in comparison to those of [25, 13], we would now understand as the onset of the shoulder in Fig. 5 as the exponential damping takes hold.

There is the same lack of doubling for short linear superconductors with open boundary conditions, where we might have thought the simple explanation had a better chance of working. However, the situation is different for short linear systems with open boundary conditions for Z_2 (rather than $U(1)$) symmetry breaking, where we seem to see doubling of the exponent in our simulations (not presented here). This is more appropriate to linear ionic crystals, giving a possible way to understand the empirical exponent doubling seen there [26].

The doubling of KZ scaling exponents for fluxon production in annular Josephson tunnel Junctions is the most complicated of all. On the one hand, it can be understood as due to the fabrication of the junction, a proximity effect arising from the (a priori undetermined) deposition of non-superconducting metal on the oxide interface. There is possibly another cause, due to the presence of a pinning centre for vortices. If we consider a short Josephson tunnel junction as an idealisation of a narrow annular junction with a strong pinning centre then the doubling effect seen in Z_2 symmetry breaking may take place here, for the Z symmetry breaking appropriate to the sine-Gordon equation in the Josephson angle θ , whose winding number counts fluxons [27]. This is under

consideration.

Note added: A similar exponential collapse of defect probability to that shown in Fig. 5 has been observed in Josephson vortices in annular condensates by Su S-W, Gou S-C, Bradley A, Fialko O and Brand J, arXiv:1302.3304. We thank J Brand for bringing this to our attention.

Acknowledgments

The authors wish to thank Arttu Rajantie for helpful discussions. RR thanks the Helsinki Institute of Physics for hospitality, where some of this work was performed. The simulations were carried out using the resources of the Imperial College High Performance Computing Service.

Appendix

For a thin-film loop, which typically has a width, w , much larger than its thickness, the intensity of the radial magnetic field, H_ρ , at the film surface, as derived from Ampere's law, is:

$$H_\rho = \frac{I_{cir}}{2w} = \frac{n\Phi_0 - \Phi_e}{2wL_{loop}}. \quad (\text{A.1})$$

In deriving the above expression we also assumed w smaller than the ring radius (or curvature radius in the case of a non-annular loop). Eq. (A.1) indicates that a superconducting loop acts as a flux-to-field transformer; if a magnetic sensor is placed above (or below) part of the loop, it will thus detect the local radial field, H_ρ , and so the magnetic flux, Φ_e , linked to the loop, and/or the winding number, n . Pannetier *et al.*[28] successfully used high-sensitivity giant magnetoresistive sensors. However, in this context, the most natural magnetic sensors are planar Josephson tunnel junctions. More specifically, the critical current of Long Josephson Tunnel Junction (LJTJ) – for which the loop itself constitutes one of the superconducting electrodes – is able to resolve flux changes well below the flux quantum [29] and promises to be a competitor of the magnetic sensors based on quantum interference [30]. Fig. A1 shows a superconducting ring acting as the base electrode for two LJTJs (the need for two LJTJs will be discussed below). Let us stress that the critical current of a LJTJ is sensitive to the surface field, H_ρ , whereas the superconducting loop is only sensitive to the perpendicular field, H_\perp .

Figs. A2 (a) and (b) show the quantum levels observed when the system is cooled through a controlled Normal-Superconducting (NS) transition in the presence of a transverse magnetic field, H_\perp , which is incremented by steps corresponding to $\sim 0.02 \Phi_0$ jumps in the freezing flux, $\Phi_f = \mu_0 H_\perp A_{loop}$, where A_{loop} is the loop area. Once H_\perp is removed, each trapped flux quantum results in a small change in H_ρ which, in turn, produces a detectable change in the junction zero-field critical current, I_c . The two panels of Fig. A2 refer to the same sample quenched in the same field range, but with

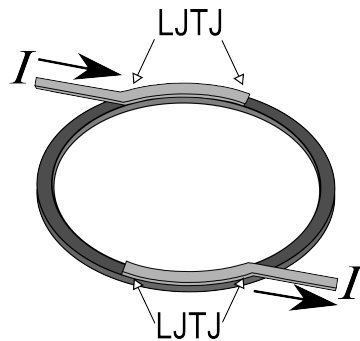


Figure A1. The magnetic field associated with the trapped fluxoids can be detected by one or more Long Josephson Tunnel Junctions, where the base electrode (dark grey) is formed by the ring itself. The top electrodes of the two planar Josephson tunnel junctions are in light grey.

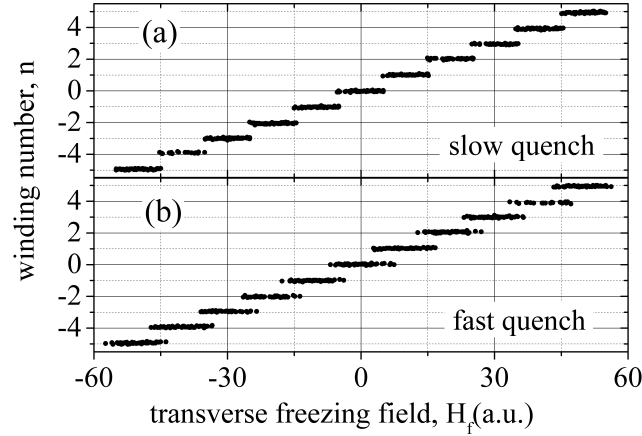


Figure A2. Winding number, n , vs. the magnetic transverse field, H_{\perp} , with which the loop was field-cooled through its superconducting transition temperature, $T_c \approx 9.1$ K. (a) slow quench: the temperature rate change, dT/dt , during the cooling through the critical temperature was -0.5 K/ms; (b) fast quench: $dT/dt \sim -50$ K/ms. Arbitrary horizontal and vertical offsets. It should be noted that H_{\perp} is switched off during the readout.

different cooling rates, dT/dt : in the first panel it is about -500 K/s, while it is hundred times larger for the second panel where a marked overlap of the quantum states is visible. This overlap is due to the non-adiabaticity of the thermal quenches and, as discussed in the main text, the quantum transition from one level to the next follows a Gaussian probability law. In deriving Figs. A2(a) and (b), we assumed that the (unknown) residual magnetic field of our setup was small enough to be trapped in the loop as less than one fluxoid. Nevertheless, the presence of any larger (static) magnetic field would simply result in a horizontal shift of the field axis or, correspondingly, a vertical shift of the winding number, n . In other words, we are able to measure the changes in the loop quantum state, but not its absolute value. Luckily, as it was argued in the main text, the transition from the n -th to the $n + 1$ -th state is virtually independent on n .

Appendix A.1. Experimental setup

Our setup consisted of a cryoprobe inserted vertically in a commercial *LHe* dewar. The cryoprobe was magnetically shielded by means of two concentric *Pb* cans and a vacuum tight cryoperm can surrounding them and immersed in the *LHe* bath ($T \simeq 4.2$ K). In addition, the measurements were carried out in an RF-shielded environment. In the experiments, we used high quality all-Niobium LJTJs fabricated on 4.2×3 mm² silicon substrates using the trilayer technique in which the Josephson junction is realized as a window opened in a *SiO*₂ insulator layer. More details on the samples electrical and geometrical parameters can be found in Ref.[29]. The chip was mounted on one side of a massive *Cu* block. Inside the outer can a *He* exchange gas with a pressure of about 20 mbar provided the thermal link between the *Cu* block and the *LHe* bath.

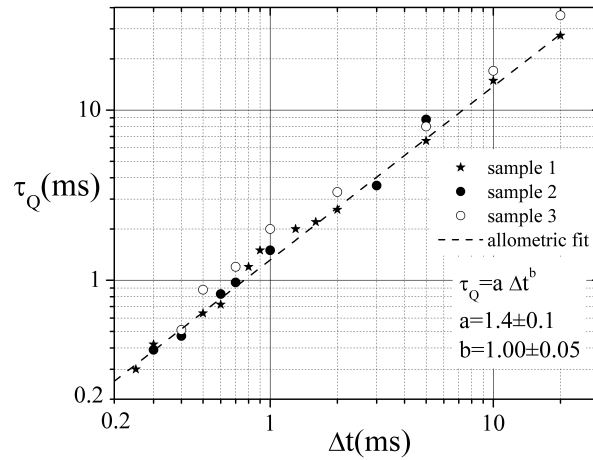


Figure A3. Quenching time, τ_Q , vs the duration, Δt , of the laser pulse for three samples. The dashed line shows the best allometric fit.

The chip was heated above the loop critical temperature, $T_c \approx 9.1$ K, by a laser beam pulse transmitted along an optical fiber down to the back side of the chip. The single crystalline Si chip absorbed a large fraction of the incident green light, and its very high thermal conductance minimized thermal gradients along the chip. After the laser pulse, the excess heat diffuses away from the chip through the thermal contact with the Cu block and the He gas inside the can; the chip temperature then relaxes down to the bath temperature.

During the transition from the normal to the superconducting states a calibrated magnetic field, H_\perp , was applied in the direction perpendicular to the loop plane by means of a superconducting cylindrical coil aligned with the loop axis, while the LJ TJ was electrically isolated: in fact, both the junction voltage and current leads were open during the whole thermal cycle. At the end of each cycle, the transverse field was removed and – as previously explained – the possible fluxoids are counted by a measurement of the LJ TJ’s (positive and negative) zero-field critical currents. Due to the annihilation of a fluxoid-antifluxoid pair, this method works well as long as the chances to have two trapped fluxoids are small. Hundreds of thermal cycles were carried out for each value of the trapping field, H_\perp ; the field value was increased in steps corresponding to about $0.1 - 0.2\Phi_0$ changes in the freezing magnetic flux, Φ_f , linked to the loop, until a total flux variation, $\Delta\Phi_f$, well above one flux quantum was achieved. In order to run batches of several thousands of equal thermal cycles with given constant parameters, the automation of thermal cycles was implemented by means of a switching unit controlled by a GPIB interface; this also allowed for much more robust statistics to be achieved. At the end of each thermal quench, the zero-field junction current-voltage characteristic is automatically digitally acquired and stored. Later, the output of each thermal cycle is analysed algorithmically to yield statistics for the trapped flux quanta.

The temperature dependence of the LJTT's gap voltage was used as an on-chip fast thermometer, to monitor the chip temperature during the thermal cycle and the quenching time, τ_Q , was inferred from a well known fitting and extrapolation procedure[31]. Fig. A3 shows that the quenching time, τ_Q , is proportional to the laser pulse duration, Δt , with the proportionality constant almost independent of the sample (and of its mounting procedure). Indeed, this method for reading the loop winding number by means of a LJTT, has been already suggested and adopted in a previous work[32], but it became reliable and efficient only when the δ -biased[33] junction was replaced by an in-line type one[34, 35, 29], as depicted in Fig. A1.

Appendix A.2. Fluxoid readout

The discrete variation, ΔI_c , of the zero-field critical current associated with each flux quantum trapped in the loop is[29]

$$\Delta I_c = g \frac{\Phi_0}{L_{loop}}, \quad (\text{A.2})$$

where g is a dimensionless parameter of the order of unity that depends on some geometrical details [29]. With a loop inductance $L_{loop} \approx 100$ pH, Eq.(A.2) provides I_c jumps of the order of several microamperes in a flux range of hundreds of flux quanta[30]. The discreteness of the critical current values is wider, when the loop is realized with a top junction electrode that, with respect to the bottom electrode, typically, has a smaller width and a larger thickness, which both result in a larger gain factor, g [36]. The validity of Eq.(A.2) has been supported by measurements on a number of devices based on narrow loops with annular and rectangular geometries, namely, rings with mean radius $R = 53 \mu\text{m}$, width $w = 6 \mu\text{m}$ and inductance $L_{loop} \sim 240$ pH and rectangular loops with mean base $b = 150 \mu\text{m}$, mean height $h = 30 \mu\text{m}$, width $w = 6 \mu\text{m}$ and inductance $L_{loop} \sim 90$ pH.

Appendix A.3. Common mode

In the common mode configuration, depicted in Fig. A1, the two LJTTs share the same doubly connected base electrode and are series biased. Any circulating current, I_{cir} , modulates oppositely the zero-field critical currents, I_{c1} and I_{c2} , of the two LJTTs; then, their difference, $\delta I_c = I_{c2} - I_{c1}$, changes twice faster with the winding number, n . Further, the rms current noise on δI_c is only $\sqrt{2}$ times larger than that on a single critical current, meaning that in the common mode configuration the signal-to-noise ratio is enhanced by a factor $\sqrt{2}$. However, the main advantage of such configuration is that by reading the two critical currents simultaneously and looking at the correlation between their changes, it is possible to exclude unwanted events from the statistical analysis. These are related to the trapping of Abrikosov vortices found at the pinning centers of the superconducting electrodes (such as normal inclusions, dislocations and grain boundaries).

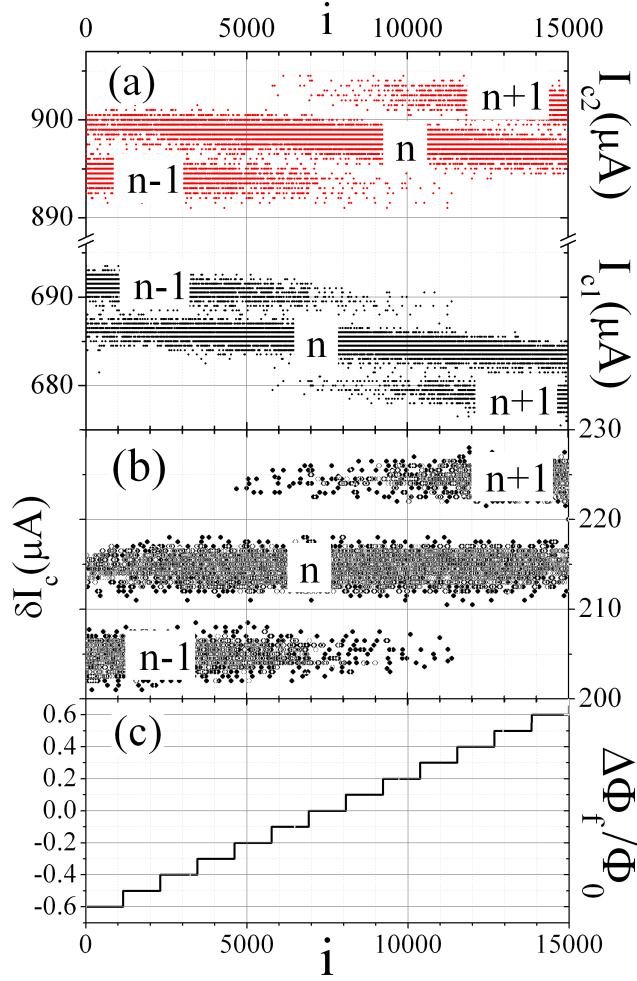


Figure A4. (a) Zero-field critical currents I_{c1} (dark points) and I_{c2} (light points) as a function of the cycle number i . (b) The same for $\delta I_c = I_{c2} - I_{c1}$. (c) Relative variation of the freezing flux, Φ_f . All plots have an arbitrary vertical offset.

When using two series-biased LJTTs, care should be taken to ensure that their critical currents are sufficiently different, otherwise the switching to non-zero voltages of the weaker junction might prematurely drive the other to the finite voltage state. One further reduction by a $\sqrt{2}$ factor of the signal-to-noise ratio is achieved by taking the combination, $I_{c2}^+ - I_{c2}^- - I_{c1}^+ + I_{c1}^-$, where $I_{c1,2}^+$ and $I_{c1,2}^-$ are the absolute values of, respectively, the positive and negative critical currents of the two LJTTs.

Appendix A.4. Measuring the trapping frequency

Fig. A4(a) shows the zero-field critical currents, I_{c1} and I_{c2} , of a two-junction annular sample during a statistical batch in which each value of the cooling field, H_\perp , was maintained for about thousand thermal cycles. Each cycle is associated with a progressive integer i , so that the index i grows linearly with time. Since each cycle lasts slightly less than 4 seconds, the total batch, consisting of 15000 cycles, required about

twelve hours. The reduction of the critical currents observed during the measurements corresponds to a small decrease (drift) of the bath temperature. The middle panel of Fig. A4 plots the difference $\delta I_c = I_{c2} - I_{c1}$; we observe that the current jumps have doubled, the signal-to-noise has been somehow lowered and, at the same time, the effect of the temperature drift has been counterbalanced. As Fig. A4(c) indicated, the cycle number i shows the step-like dependence of the freezing flux, Φ_f , as time goes by. Let us call Φ_r the residual magnetic flux; then, to reproduce the zero-flux condition during the quench, a freezing flux $\Phi_f = -\Phi_r$ needs to be applied. Since Φ_r is, in general, unknown, it is necessary to span Φ_f over a range at least as large as one flux quantum.

From the statistical analysis of data this obtained – such as that shown in Fig. A4(b) – it is possible to determine the frequency distributions, f_m . In order to compare loops with different effective area, the trapping frequency, f_m , is plotted against the normalized freezing magnetic flux, $\phi_f \equiv \Phi_f/\Phi_0$, rather than the freezing field, H_\perp . Two examples of the computed frequency distributions were given in the main text in Figs. 7(a) and (b); the statistical data are very nicely fit by a Gaussian behavior, as in Eq.(37).

References

- [1] Kibble T W B 1976 *J. Phys.* **A9** 1387
- [2] Kibble T W B 1980 *Physics Reports* **67** 183
- [3] Zurek W H 1985 *Nature* **317**, 505
- [4] Zurek W H 1996 *Physics Reports* **276** 177
- [5] Karra G and Rivers R J 1997 *Phys. Lett. B* **414** 28
- [6] Karra G and Rivers R J 1998 *Phys. Rev. Lett.* **81** 3707
- [7] Weir D J and Rivers R J 2011 *J. Phys.: Conf. Ser.* **286** 012056
- [8] Weir D J, Monaco R and Rivers R J 2013, to appear in *J. Low Temp. Phys.*
Preprint arXiv:1208.3426
- [9] Antunes N D, Gandra P and Rivers R J 2006 *Physical Review D* **73**, 125003
- [10] Laguna P and Zurek W H 1997 *Phys. Rev. Lett.* **78** 2519;
Yates A and Zurek W H 1998 *Phys. Rev. Lett.* **80** 5477
- [11] Antunes N D, Bettencourt L M A and Zurek W H 1999 *Phys. Rev. Lett.* **82** 2824
- [12] Bettencourt L M A, Antunes N D and Zurek W H 2000 *Phys. Rev.* **62** 065005
- [13] Monaco R, Mygind J, Aaroe M, Rivers R J and Koshelets V P 2006 *Phys. Rev. B* **74** 144513
- [14] Rivers R J, Monaco R, Mygind J, Aaroe M and Koshelets, V P 2008 *Phil. Trans. R. Soc. A* **366** 2871
- [15] Monaco R, Aaroe M, Mygind J, Rivers R J and Koshelets V P 2008 *Phys. Rev. B* **77** 054509
- [16] Rivers R J 2001 *Jour. Low Temp. Phys.* **124** 41
- [17] Borrill J and Gleiser M 1997 *Nucl. Phys. B* **483** 416
- [18] Rivers R J, Kavoussanaki E and Karra G 2000 *Cond. Mat. Phys.* **3** 133
- [19] Hindmarsh M and Rajantie A 2000 *Phys. Rev. Lett.* **85** 4660
- [20] Rajantie A 2001 *Jour. Low Temp. Phys.* **124** 5
- [21] Halperin B I 1981, published in *Physics of Defects*, proceedings of Les Houches, Session XXXV 1980 NATO ASI, editors Balian, Kléman and Poirier (North-Holland Press, 1981) 816.
- [22] Liu F and Mazenko G F 1992 *Phys. Rev. B* **46** 5963
- [23] Monaco R, Mygind J, Rivers R J and Koshelets V P 2009 *Phys. Rev. B* **80** 180501
- [24] Krasnitz A 1995 *Nucl. Phys. B* **455** 320
- [25] Monaco R, Mygind J, Aaroe M, Rivers R J and Koshelets V P 2006 *Phys. Rev. Lett.* **96**, 080604

- [26] Pyka K, Keller J, Partner H L, Nigmatullin R, Burgermeister T, Meier D-M, Kuhlmann K, Retzker A, Plenio M B, Zurek W H, del Campo A and Mehlstäubler T E 2011 *Preprint* arXiv:1211.7005
- [27] Gordeeva A V and Pankratov A L 2010 *Phys. Rev. B* **81**, 212504
- [28] Pannetier M, Fermon C, Le Goff G, Simola J, Kerr E, *Science*, **304**, 1648 (2004);
Pannetier M, Fermon C, Le Goff G, Simola J, Kerr E, Welling M, and Wijngaarden RJ, *IEEE Trans. on Appl. Supercond.* **15**, 892 (2005).
- [29] Monaco R, Mygind J, and Koshelets VP, *Phys. Rev. B* **85**, 094514 (2012).
- [30] Monaco R, *Supercond. Sci. Technol* **25**, 115011 (2012).
- [31] Monaco R, Aaroe M, Mygind J, Rivers RJ, and Koshelets VP, *Phys. Rev. B* **74**, 144513 (2006).
- [32] Monaco R, Mygind J, Rivers RJ, and Koshelets VP, *Phys. Rev. B* **80**, 180501(R) (2009);
John R. Kirtley and Francesco Tafuri, *Physics* **2**, 92 (2009).
- [33] Monaco R, Mygind J, Koshelets VP and Dmitriev P, *Phys. Rev. B* **81**, 054506 (2010).
- [34] Ferrel RA and Prange RE, *Phys. Rev. Lett.* **10**, 479 (1963).
- [35] Owen CS and Scalapino DJ, *Phys. Rev.* **164**, 538 (1967).
- [36] Monaco R, Koshelets VP, Mukhortova A and Mygind J, private communication;
idem, *Preprint* arXiv:1301.1274